Journal of Alloys and Compounds 537 (2012) 65–70

Contents lists available at SciVerse ScienceDirect

Journal of Alloys and Compounds

journal homepage: www.elsevier.com/locate/jalcom

Effect of Nb and W substitutions on the stability of the A15 Mo_3Si phase

P.K. Ray *, Y.Y. Ye, M. Akinc, M.J. Kramer

Ames Laboratory and Department of Materials Science and Engineering, Iowa State University, Ames, IA 50011, United States.

ARTICLE INFO

Article history:
Received 28 February 2012
Received in revised form 20 April 2012
Accepted 23 April 2012
Available online 8 May 2012

Keywords:
Intermetallic compounds
Silicides
Phase transformations

ABSTRACT

A combination of theoretical and experimental studies on the stability of Mo_3Si with Nb and W substitutions has been presented in this paper. The first principles calculations suggest that the formation enthalpy of the A15 phase favors Nb substitution up to 37.5 atom %. In case of W substitution, the formation enthalpies increase monotonically. Experimental studies on the other hand, showed that the A15 phase is destabilized when approximately 27.5 atom % Nb is added while 7.5–10 atom % W substitution was sufficient to destabilize A15 phase. It was further determined that upon destabilization of the A15 structure, Nb partitions preferentially to the T1 phase, whereas W partitions preferentially to a solid solution with Mo.

1. Introduction

The drive for greater energy efficiencies requires the modern day gas turbines to operate at as high a temperature as possible, in highly oxidative environments. This has been a key driver for the development of novel alloys that can withstand such harsh conditions. Ni based superalloys have been the workhorse material for the high temperature industry for several decades. However, these alloys are intrinsically restricted to temperatures under 1050 °C due to their relatively low melting temperatures [1]. Refractory metal silicides have long been known to have high melting temperatures, and in some cases, excellent oxidation resistance [2–9]. These properties have been exploited in $MoSi_2$ based alloys for a variety of applications like heating elements in furnaces. Subsequently, molybdenum silicides have also emerged as an attractive candidate for ultra-high temperature applications [10–12]. The oxidative stability of these alloys, especially compositions with relatively low Si content, has been further improved by controlled boron substitution. Boron doped Mo_5Si_3 has been shown to form a borosilicate scale that provides excellent oxidation resistance at high temperatures [5–9,13,14]. However, the oxidation resistance of these materials is largely due to the presence of intermetallic phases that also happen to be brittle [15]. In order to develop adequate ductility and toughness along with oxidation resistance, it becomes essential to have a metal rich solid solution phase in thermodynamic equilibrium with these intermetallics, i.e., a two phase microstructure consisting of a Mo rich solid solution and the $Mo_5Si_3B_x$ compound. The improvement in mechanical properties due to the presence of a continuous Mo rich solid solution has been demonstrated earlier [16].

In the Mo–Si binary phase diagram [17], Mo_3Si exists between the Mo and the Mo_5Si_3 phase as A15 Pm-3n phase. The Mo_3Si phase is also present in the Mo–Si–B ternary when the Mo rich solid solution and the T2 Mo_5SiB_2 phase exist in thermodynamic equilibrium [18,19]. Studies on the Mo–Si–B ternary system indicates that boron solubility in the A15 phase is minimal up to 1800 °C [20]. The amount of Si in Mo_3Si is not sufficient to form a completely hermetic oxide scale and protect the alloy. Consequently, this phase has very poor oxidation resistance [21–23]. The A15 phase is also undesirable due to its very low fracture toughness as a result of having very few active slip systems [24]. Studies on Mo–Nb–Si–B alloys indicate that the A15 phase can be removed from the microstructure if a large amount of Nb is added to the alloy [25,26]. This has been further corroborated thermodynamically using an extension [27] of the semi-empirical Miedema model [28–35] for multicomponent alloys. However, it has also been demonstrated that the substitution of Nb adversely affects the oxidation resistance [25,26]. Hence, it is important to destabilize the A15 phase with the minimum amount of Nb. In addition to Nb, W substitution can also destabilize the A15 phase, given the absence of a W_3Si phase in the W–Si phase diagram. Therefore, in this paper we compare the effects of Nb and W substitution on the stability of A15 Mo_3Si phase.

2. Theoretical calculations

The first principles calculations were carried out in the present work using the Vienna *ab initio* simulation package (VASP) within the framework of the density functional theory (DFT). The calculation is conducted in a plane-wave basis, using the

* Corresponding author. Tel.: +1 515 294 4064; fax: +1 515 294 5444.
E-mail address: prat@iastate.edu (P.K. Ray).

0925-8388/$ - see front matter © 2012 Published by Elsevier B.V.
http://dx.doi.org/10.1016/j.jallcom.2012.04.109

projector-augmented wave (PAW) method with ultra-soft pseudopotentials [36]. The exchange and correlation items are described by the generalized gradient approximation (GGA), and the cutoff energies are 320 and 535 eV for the plane wave basis and augmentation charge respectively. During the relaxation calculation, the energy criteria are 0.01 and 0.1 meV for electronic and ionic relaxations respectively, while for calculation of the density of states (DOS), the criterion is 0.001 meV. The *k*-point grid used for structural relaxation was $6 \times 6 \times 6$, chosen according to the Monkhorst–Pack scheme [37], and symmetry reduced to the irreducible Brillouin zone. The calculations for the M_3Si ($M = Mo_{1-x}Nb_x$ or $M = Mo_{1-x}W_x$) phase were carried out using a super cell of the A15 structure of *z* M atoms and *y* Si atoms across the entire range of *x*. The amounts of Nb and Mo as well as W and Mo were varied to calculate the formation enthalpies. The DOS for this structure was also calculated as a function of Nb content.

3. Experimental methods

Alloys were synthesized by arc-melting of pure elemental chips (Alfa Aesar, +99.5%) on a water cooled copper hearth in an inert argon atmosphere. The alloy buttons were re-melted a minimum of four times in order to ensure adequate homogeneity. In addition to the pure Mo_3Si, five alloys were cast in the Mo–Nb–Si system, having compositions $Mo_{75-x}Nb_xSi_{25}$ (with $x = 10$, 20, 25, 27.5 and 30). The high melting temperature of W resulted in minor W segregation initially. This problem was overcome by adopting a two-stage synthesis process. In the first stage, WSi_2, having a relatively low melting temperature (2160 °C) was cast and remelted thrice. In the second stage, the WSi_2, along with the balance W, Si and Mo was cast and remelted four times. Five alloys having compositions $Mo_{75-y}W_ySi_{25}$ ($y = 2.5$, 5, 7.5, 10, 12.5 and 15) were cast in this system. The alloys were heat treated at 1850 °C in an atmosphere of flowing ultra-high purity argon in tantalum containers. The heating as well as the cooling rates were controlled at 20 °C/min.

Microstructures of the alloys were studied using a JEOL 5910LV scanning electron microscope at an accelerating voltage of 20KV. Phase analyses of the alloys were carried out using a Philips PANalytical X-ray diffractometer with a Bragg–Brentano geometry using a monochromatic Cu Kα radiation (wavelength = 1.54059 Å) with a step size of 0.0167°. The X-ray data was then Rietveld refined using GSAS [38] to quantify the change in lattice parameters of various phases due to Nb or W substitution for Mo and to estimate the relative amounts of different phases present in the sample. Substitutionally, wavelength-dispersive spectra (WDS) were recorded on the A15 grains to estimate the Nb and W substitution in these alloys. Approximately 100 points were collected for each sample using automated data analysis. The WDS measurements were carried out using JEOL JXA-8200 microprobe. Data was acquired at an accelerating voltage of 20 KV, with a beam current of 20 nA. Si–K_α, Mo–L_α and Nb–L_α lines were used for analysis. A counting time of 10 s on the peak and 5 s on the background on either side of the peak was used.

4. Results and discussion

4.1. Effect of Nb substitution

Behrani et al. showed that the A15 phase can be destabilized due to Nb substitution in a Mo–Nb–Si–B quaternary alloy [25]. However, experimental assessment of critical composition in a quaternary system involves a significant amount of Edisonian trials. Lack of thermodynamic databases in the Nb–B system also renders a computational assessment of the quaternary system an unviable task. However, the lack of boron solubility in the A15 structure allows us to explore the ternary Mo–Nb–Si or Mo–W–Si in order to assess the critical amount of substitution to the Mo–Si system in order to remove the A15 phase from the microstructure. Recent calculations by Geng et al. [39] indicated a finite phase width of the Mo_3Si phase with Nb substitution, beyond which a three-phase region comprising of a bcc Mo based solid solution, the A15 $(Mo,Nb)_3Si$ and the T1 $(Mo,Nb)_5Si_3$ phase should form. Our experimental work presented in this paper and previous calculations using an extension of the semi-empirical Miedema's model [27] agree well with these results in terms of the critical amount of Nb substitution required for destabilization of the A15 phase. However, the three phase region appears to have a slightly narrower phase width than predicted by Geng et al. [39].

Fig. 1 shows the variation of formation enthalpy of $(Mo,Nb)_3Si$ in the A15 structure from our *ab initio* calculations. In order to check the accuracy of the calculations, the formation enthalpy values estimated using the *ab initio* calculations were compared with the experimentally determined values available in the literature. Fujiwara and Ueda estimated a value of $-122.1 + 0.0027T \pm 0.15$ kJ/mol [40] while Tomaszkiewicz et al. estimated a value of -125 ± 5.8 kJ/mol from fluorometric calorimetry at 298 K [41]. These experimental results compare favorably with the values obtained from first principles calculations in this work (−134.8 kJ/mol). The trends in formation enthalpy seen in our calculations can be understood on the basis of thermodynamic considerations, and this has been discussed below.

For the purpose of this discussion, we shall use the data available from the work of Miedema and his coworkers [33–35]. Miedema described the interactions occurring at the interface of the Wigner–Seitz cell of an element being solved in another using an interfacial enthalpy term [30,33,34], which is a function of the electronegativity difference between the elements and the difference in the electron density at the Wigner–Seitz cell boundary of the elements. This term has a parallel in the interaction parameter as it is defined in the CALPHAD approach. Essentially, this is a measure of the strength of interaction between two atoms when brought together. This value, for solvation of Si in Mo was determined to be −120 kJ/mol of Si, whereas the corresponding value for solvation of Si in Nb was determined to be −195 kJ/mol [33–35]. Similarly, the interfacial enthalpy for solvation of Mo in Si is −126 kJ/mol of Mo while that for solvation of Nb in Si is −216 kJ/mol of Nb [33–35]. Therefore, the Nb–Si interaction is stronger compared to the Mo–Si interaction. With increasing levels of Nb substitution at the expense of Mo content, the contribution of Nb–Si interactions becomes more significant as compared to the Mo–Si interactions. In addition to the Mo–Si and Nb–Si interactions, Mo–Nb interactions need to be considered as well. The interfacial enthalpy values estimated for solvation of Mo in Nb is −22 kJ/mol of Mo, while the corresponding value for Nb in Mo is −23 kJ/mol of Nb. This metal–metal interaction is significantly weaker than the two metal–metalloid interactions. Consequently, initial Nb substitution serves to stabilize the Mo_3Si compound as evidenced by an initial reduction in formation enthalpy estimated from the *ab initio* calculations (see Fig. 1). However, once the number of Nb–Si pairs get saturated, further substitution of Nb leads to Nb–Nb interactions replacing the Mo–Nb interactions, which, by definition have interfacial enthalpy of zero. Consequently, an

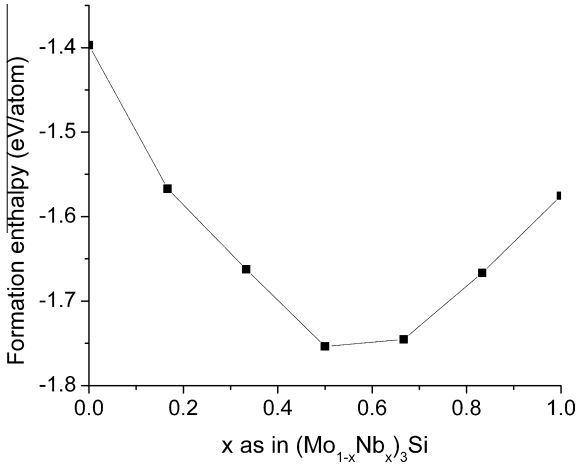

Fig. 1. Variation of formation enthalpy with increasing Nb additions at 0 K.

increase in the formation enthalpy is predicted. Since the Nb–Si interactions are stronger than the Mo–Si interactions and much stronger than the Mo–Nb interactions, the increase in formation enthalpy beyond a critical Nb content occurs with a slope that is shallower than the slope observed during the initial decrease in the formation enthalpy. This is in fact observed in our *ab-initio* calculations (Fig. 1), where an initial decrease in the formation enthalpy followed by an increase. This would indicate an initial stabilization of the A15 compound followed by a subsequent destabilization beyond a certain level of Nb substitution.

In these multicomponent systems care is needed in assessing the different possible phase selections. In this case, the binary phase diagrams would suggest that should the A15 get destabilized, it would decompose into a metal rich solid solution and the $(Mo,Nb)_5Si_3$, T1 phase. With increasing Nb substitution, the partitioning of the metals into the competing phases will have to be taken into consideration. In case of the metal rich solid solution, an increase in Nb content should result in the increase in the number of Mo–Nb interactions at the cost of Mo–Mo interactions. The Mo–Nb interactions have lower energy and should result in increasing the stability of the solid solution with respect to one having a lower Nb content. Therefore, an increase in Nb substitution would further stabilize the solid solution. Similarly, an increase in the Nb substitution at the cost of Mo will increase the number of Nb–Si interactions with a corresponding decrease in the number of Mo–Si interactions. As in Mo–Nb solid solution, this would stabilize the T1 phase. It has been shown by McMahan et al. that the number of metal–metal bonds per atom is higher in the A15 structure than the T1 structure, whereas the number of metal–silicon bonds per atom is higher for the T1 structure as opposed to the A15 structure [42]. This would indicate that the stabilization effect due to Nb substitution is much more prominent for the T1 structure as compared to the A15 structure even in the initial stage. Consequently, it would be expected that beyond a critical level of substitution, due to increasing stabilization of the T1 phase and the solid solution vis-à-vis the A15, the single phase A15 would decompose to form T1 and the solid solution.

In substitution to the estimation of formation enthalpies, density of states plots were calculated for different levels of Nb substitution. These plots are shown in Fig. 2. The location of the Fermi surface on a DOS plot provides some indications on the structural stability of these compounds. It can be seen that at the enthalpy minima, the Fermi surface has moved out of the gap at the equiatomic Mo:Nb ratio. This would suggest that there is a possibility for the structure to be unstable at this composition level despite the lowering of formation enthalpy.

Fig. 3 shows the X-ray diffraction patterns for different compositions. The diffraction pattern at the bottom of the stack corresponds to the single phase pure Mo_3Si. The refined lattice parameter of the Mo_3Si was found to be 4.8921 Å which is in good agreement with the values reported in the literature [17,43]. As Nb is added to the system, a systematic shift of the Mo_3Si peaks towards the lower 2θ values can be seen, indicating an increase in the lattice parameters as expected, since Nb is slightly larger than Mo (2.08 Å vs. 2.01 Å). It is also clear that as we move from $Mo_{50}Nb_{25}Si_{25}$ to $Mo_{47.5}Nb_{27.5}Si_{25}$, the single phase A15 structure decomposes to form a two phase mixture comprising of a Mo-based solid solution and the T1 $(Mo,Nb)_5Si_3$ phase. Even at a lower $Mo_{50}Nb_{25}Si_{25}$ alloy composition, minor traces of T1 $(Mo,Nb)_5Si_3$ and the Mo solid solution can be observed in the diffraction pattern. Refinement of the diffraction pattern of the alloy with nominal composition $Mo_{47.5}Nb_{27.5}Si_{25}$ showed a presence of a minor amount of the A15 (<5%). Phase analysis of $Mo_{45}Nb_{30}Si_{25}$ failed to show any A15 phase. This would seem to indicate that the three phase region is extremely narrow, ~27.5–30% of Nb substitution along the Mo_3Si–Nb_3Si tie-line, which is slightly narrower than

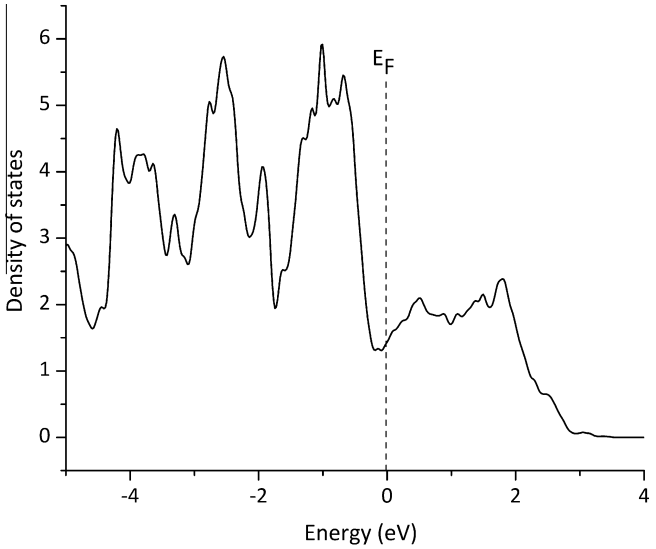

Fig. 2. Density of states of $Mo_{1.5}Nb_{1.5}Si$.

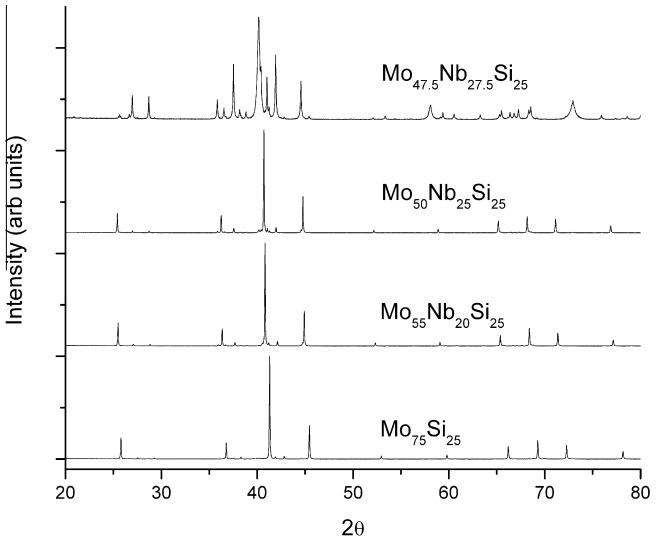

Fig. 3. X-ray diffraction patterns from selected compounds in the Mo–Nb–Si series of alloys.

the values obtained by Geng et al. [39]. In substitution to the formation enthalpy and density of states, the *ab initio* calculations were also used to calculate the lattice parameters of the Mo_3Si compound with increasing Nb substitution. The results obtained from the first principles calculations were compared with experimental results in order to verify the accuracy of the calculations. Table 1 shows the lattice parameters obtained from first principles calculations and experimentally determined values. The agreement between calculated and observed lattice parameters is excellent which provides further evidence for larger Nb is occupying only the Mo site.

Fig. 4 shows the microstructures of the alloys with and without the A15 phase. When A15 is stable, it approached 100% of the sample allowing accurate compositional analysis by WDS. These measurements confirmed that the composition of the A15 phase in each case was close to the target compositions. Since Mo_3Si is a line compound and Mo has some Si solubility, marginal compositional variations during melting are quite likely, leading to the formation of small amount of other phases. As the molten alloy cools down, it

Table 1
Comparison of the A15 lattice parameters determined experimentally and from first principles.

Alloy	Experimental value (Å)	First principles (Å)
Mo_3Si	4.8921	4.89
$Mo_{2.5}Nb_{0.5}Si$	4.9443	4.95
Mo_2NbSi	4.9812	4.98

first passes through the liquidus resulting in the formation of a minor amount of the Mo rich solid solution. The remaining liquid along with the Mo solid solution that was already formed solidifies following a peritectic reaction path resulting in formation of the Mo_3Si compound [44]. In the higher Nb content alloy, where the Mo_3Si is unstable, the solidification follows a different path, with an eutectic microstructure evolving in place of the peritectic solidification product resulting in a two phase mixture of Mo based solid solution and the $(Mo,Nb)_5Si_3$ phase. Fig. 4a shows a region having a small amount of the T1 $(Mo,Nb)_5Si_3$ phase embedded in a Mo_3Si matrix. It is quite clear from the micrograph that Mo_3Si is still the primary solidification phase. Fig. 4b shows a two phase mixture of Mo rich solid solution (bright) and the $(Mo,Nb)_5Si_3$ phase (dark) once the A15 phase is destabilized.

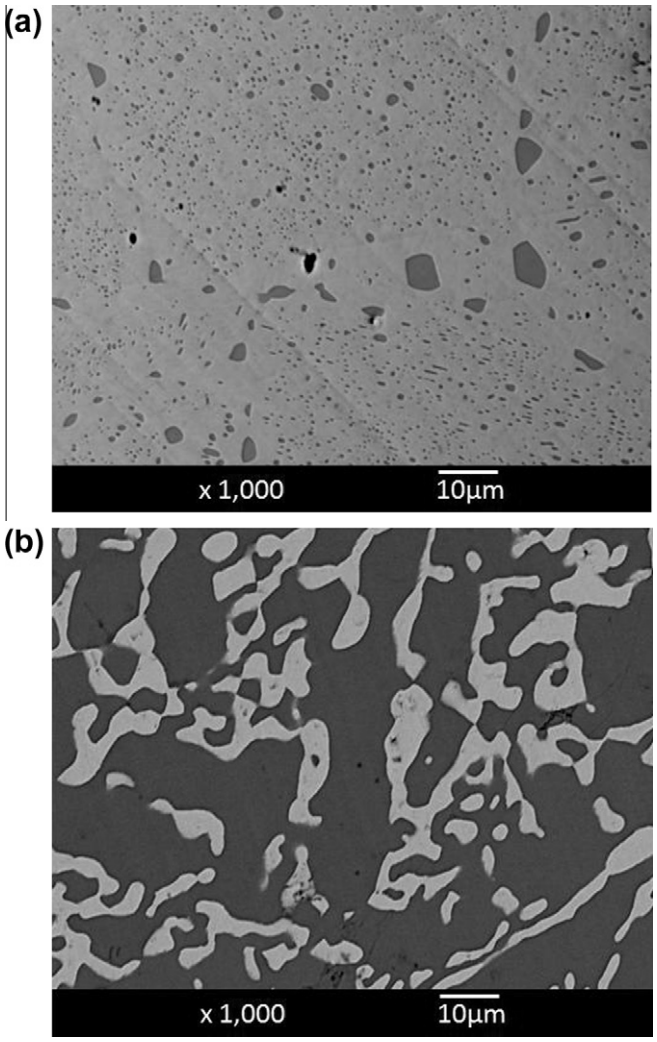

Fig. 4. Microstructures of Mo–Nb–Si alloys. (a) Alloys with the composition $Mo_{25}Nb_{25}Si_{25}$ have a largely single phase microstructure with very small amounts of b.c.c. Mo solid solution phase and the T1 $(Mo,Nb)_5Si_3$ phase. (b) Alloys with the composition $Mo_{45}Nb_{30}Si_{25}$ show an exclusively two phase microstructure consisting of the Mo rich solid solution and the T1 phase.

The lattice parameters as a function of Nb content were determined by Rietveld refinement of the powder X-ray data and showed a linear increase consistent with the Vegard's law since Nb forms an isomorphous solid solution with Mo. The Vegard's law can be used to determine the actual fraction of Nb in the A15 phase using the lattice parameter of 5.15 Å for A15 Nb_3Si [45]. The compositions determined from Rietveld refinement and WDS are in fairly good agreement. Microprobe analysis of the T1 phase in the multiphase alloys showed that the T1 phase had an equiatomic Mo:Nb ratio, which would correspond to a Nb level that is much higher than the nominal composition, thereby indicating a preferential partitioning of the Nb to the T1 intermetallic as opposed to the metal rich solid solution.

4.2. Effect of W substitution

The interfacial enthalpy for solvation of Si in W has been reported as −102 kJ/mol whereas the corresponding value for solvation of W in Si has been reported as −110 kJ/mol [33–35]. This would indicate that W–Si interactions are weaker than Mo–Si interactions (−120 and −126 kJ/mol respectively). Substitutionally, the interfacial enthalpy for solvation of Mo in W, as well as that of W in Mo has been reported as −1 kJ/mol [33–35]. Therefore, W substitution resulting in W–Si interactions at the expense of Mo–Si interaction will only serve to raise the formation enthalpy of the A15 compound. The Mo–W interactions are only slightly stronger than the Mo–Mo interaction; hence the slight decrease in formation enthalpy due to an increase in Mo–W interactions will be far outweighed by the significant increase in formation enthalpy due to the increased number of weaker W-Si interactions. Therefore, in this case, unlike the Mo–Nb–Si system, a monotonic increase in formation enthalpy is to be expected.

Fig. 5 shows the variation of formation enthalpy with W substitution. It can be seen that W substitution does in fact result in a strictly monotonic increase in the formation enthalpy. With progressive W substitution, the two competing phases would be the Mo–W solid solution and the $(Mo,W)_5Si_3$ T1 phase. Using similar arguments as above, it would appear that W substitution would not reduce the formation enthalpy of either of these phases. However, the phase assemblage could still be more stable than the A15 structure if W preferentially partitioned into the solid solution, leaving only a relatively small amount of W available to substitute for Mo in the T1 phase. In such an event, the T1 structure would still contain a fairly large amount of Mo–Si interactions in comparison to the A15 phase resulting in the destabilization of the A15

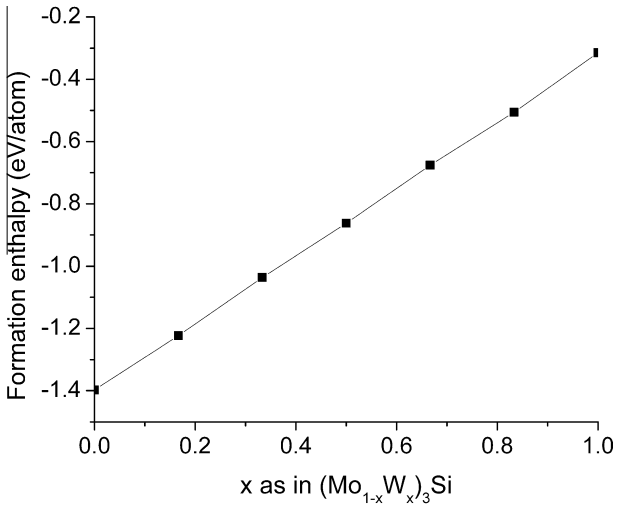

Fig. 5. Variation of formation enthalpy of A15 with increasing W additions at 0 K.

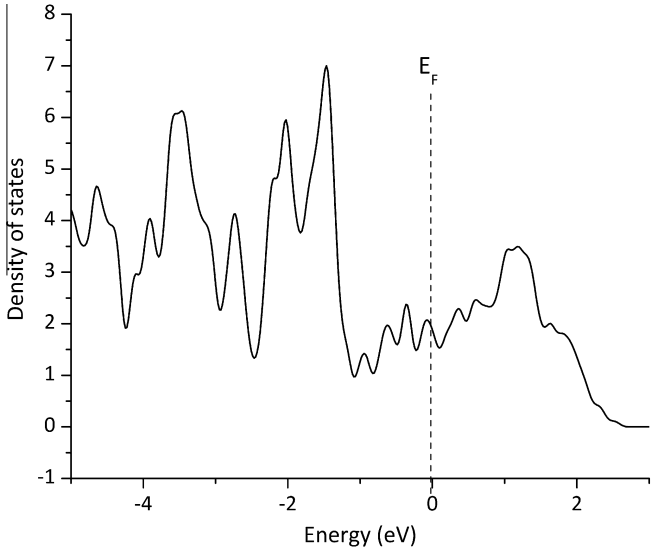

Fig. 6. Density of states of $Mo_{62.5}W_{12.5}Si_{25}$.

structure. As will be discussed later, the microprobe and XRD work supports the above assertion. This, combined with the W–Si phase diagram [46] would suggest that beyond a certain amount of W substitution, the A15 phase is likely to become destabilized.

Fig. 6 shows the density of states of the $Mo_{62.5}W_{12.5}Si_{25}$ alloy. It can be seen that at this composition the Fermi surface has moved out of the pseudo-gap suggesting that the structure might be unstable at this composition. As with the previous set of Mo–Nb–Si alloys, we use these calculations as a guide for selecting experimental compositions rather than for making any conclusive comments on the phase stability. These results indicated that the A15 structure might be destabilized with a much smaller level of W substitution compared to Nb. Hence, the experimental studies were focused largely in the lower W substitution levels.

Fig. 7 shows the X-ray diffraction patterns with different levels of W substitution. The diffraction pattern at the bottom of the sequence corresponds to zero W substitution, i.e. the pure A15 Mo_3Si phase. As the level of W substitution is increased, it can be seen that additional peaks that belong to the $(Mo,W)_5Si_3$ phase (T1) and the (Mo,W) solid solution starts to appear. The signature peaks

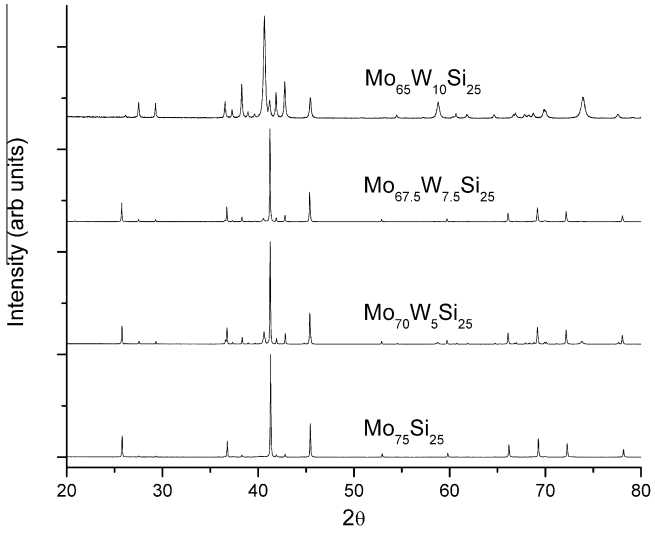

Fig. 7. X-ray diffractograms with progressively increasing W content.

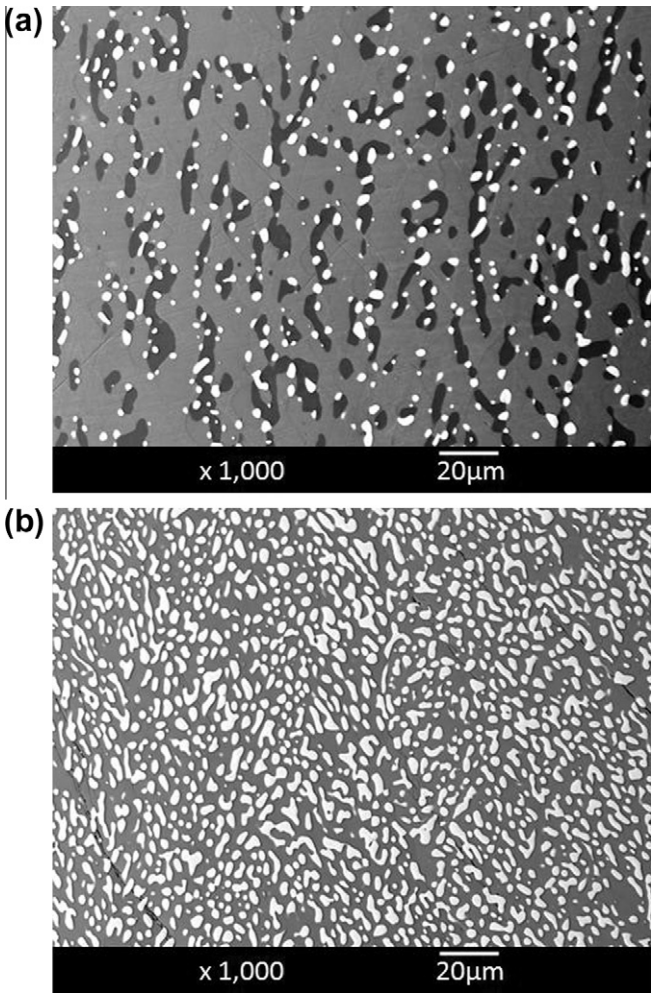

Fig. 8. SEM micrographs of Mo–W–Si alloys. (a) Microstructure of a $Mo_{67.5}W_{7.5}Si_{25}$ alloy, (b) Microstructure of a $Mo_{60}W_{15}Si_{25}$ alloy.

for Mo_3Si at $2\theta = 26°$ and 41° disappear at ~10 atom % W substitution, indicating the absence of the A15 phase from the alloy. At this stage, the signature peaks of the T1 phase at $2\theta = 27°$, 29°, 38° and 43° can be observed instead. Additionally, a peak at $2\theta = 40.5°$ corresponding to the most intense peak of Mo can be seen. The lattice parameters of the W substituted compounds were determined via Rietveld refinement. The increase in lattice parameter is almost linear, in accordance with Vegard's law. Microprobe analyses on these samples indicate a maximum W content of 7 atom %. Such a result, along with the diffractograms shown in Fig. 7 would indicate that W solubility in the A15 structure is in the 7–10 atom % range; substitution beyond this level leads to the decomposition of the A15 phase to form a mixture of the Mo rich solid solution and the T1 $(Mo,W,)_5Si_3$ phase.

Microprobe analysis carried out on the two phase alloy with 15% W indicated approximately 26% W in the metal rich solid solution (remainder being 70% Mo and 4% Si). W composition in the T1 $(Mo,W)_5Si_3$ on the other hand, was found to be under 5%. This corresponds to a 12:1 Mo:W ratio in the T1 phase and approximately 3:1 Mo:W ratio in the metal rich solid solution. This confirms the hypothesis that W preferentially partitions to the solid solution rather than the T1 intermetallic compound. Fig. 8a shows a micrograph of an alloy with 7.5 atom % W substitution. According to the X-ray diffraction patterns, this alloy is comprised largely of single phase $(Mo,W)_3Si$. This fact is further corroborated by the micrograph which shows a gray matrix of $(Mo,W)_3Si$ with smaller phase features embedded in it. The bright phase was determined to

be a (Mo,W) solid solution using WDS whereas the darker features were identified to be the $(Mo,W)_5Si_3$ phase. Fig. 8b shows the microstructure of $Mo_{60}W_{15}Si_{25}$ alloy. The X-ray diffraction patterns revealed almost complete removal of the A15 phase from this alloy resulting in a phase mixture of a metal rich solid solution and the T1 phase. The microstructure indeed confirms this with the bright phase being the (Mo,W) solid solution and the dark phase being identified as the $(Mo,W)_5Si_3$ T1 phase.

5. Conclusions

The phase stability is dictated by chemical potential, rather than formation enthalpy alone. However, the enthalpy of formation can still be a useful indicator in understanding the stability. In the present work, *ab-initio* calculations were used as a guideline for designing experiments to study the phase stability of the A15 phase with Nb or W substitution. The experimental results were in good agreement with the computational studies. In both cases, with W and Nb additions, it was seen that the A15 phase followed Vegard's law over the composition range it exists. It was shown that both Nb and W substitution destabilize the A15 phase beyond a certain critical level of substitution. Additionally, the X-ray diffraction patterns and microprobe analyses suggest that although the A15 phase gets destabilized completely beyond a critical amount of Nb and W, at lower levels of substitution, a three phase field consisting of the solid solution, T1 and A15 is present. In case of Nb substitution, it was seen that 27.5 atom % substitution is required to eliminate the A15 phase entirely. This result is consistent with the calculations by Geng et al. [39]. In case of Mo–W–Si alloys, 10 atom % W substitution was sufficient to eliminate the A15 phase from the microstructures.

Acknowledgements

This work was supported by the AFOSR HTAM under the contract # FA9550-11-1-201.

References

[1] R.C. Reed, The Superalloys: Fundamentals and Applications, Cambridge University Press, Cambridge, 2006.
[2] J. Perepezko, R. Sakidja, JOM Journal of the Minerals, Metals and Materials Society 62 (2010) 13–19.
[3] J.S. Park, R. Sakidja, J.H. Perepezko, Scripta Materialia 46 (2002) 765–770.
[4] R. Sakidja, J.S. Park, J. Hamann, J.H. Perepezko, Scripta Materialia 53 (2005) 723–728.
[5] M. Meyer, M. Kramer, M. Akinc, Advanced Materials 8 (1996) 85–88.
[6] M.K. Meyer, A.J. Thom, M. Akinc, Intermetallics 7 (1999) 153–162.
[7] M.K. Meyer, M. Akinc, Journal of the American Ceramic Society 79 (1996) 938–944.
[8] K. Yoshimi, S. Nakatani, S. Hanada, S-H. Ko, Y.H. Park, Science and Technology of Advanced Materials 3 (2002) 181–192.
[9] N. Nomura, T. Suzuki, K. Yoshimi, S. Hanada, Intermetallics 11 (2003) 735–742.
[10] M. Yamaguchi, H. Inui, K. Ito, Acta Materialia 48 (2000) 307–322.
[11] D.M. Dimiduk, J.H. Perepezko, MRS Bulletin 28 (2003) 639–645.
[12] J.J. Petrovic, A.K. Vasudevan, Materials Science and Engineering A 261 (1999) 1–5.
[13] S.C. Okumus, M.J. Kramer, A.J. Thom, M. Akinc, Key Engineering Materials 264-268 (2004) 509–512.
[14] A.J. Thom, E. Summers, M. Akinc, Intermetallics 10 (2002) 555–570.
[15] D.L. Anton, D.M. Shah, Materials Research Society Symposium Proceedings 213 (1991) 733–738.
[16] M. Kruger, S. Fraanz, H. Saage, M. Heilmaier, J.H. Schneibel, P. Jehanno, M. Bonning, H. Kestler, Intermetallics 16 (2008) 933–941.
[17] A.B. Gokhale, G.J. Abbaschian, Journal of Phase Equilibria and Diffusion 14 (1991) 493–498.
[18] O. Hassomeris, G. Schumacher, M. Kruger, M. Heilmaier, J. Banhart, Intermetallics 19 (2011) 470–475.
[19] T. Depkas, Ch. Somsen, G. Eggeler, D. Mukherjee, J. Rosler, M. Kruger, H. Saage, M. Heilmaier, Materials Science and Engineering: A 510–511 (2009) 337–341.
[20] J.J. Huebsch, M.J. Kramer, H.L. Zhao, M. Akinc, Intermetallics 8 (2000) 143–150.
[21] I. Rosales, H. Martinez, D. Bahena, J.A. Ruiz, R. Guardian, J. Colin, Corrosion Science 51 (2009) 534–538.
[22] F.A. Rioult, S.D. Imhoff, R. Sakidja, J.H. Perepezko, Acta Materialia 57 (2009) 4600–4613.
[23] S. Ochiai, Intermetallics 14 (2006) 1351–1357.
[24] I. Rosales, J.H. Schneibel, L. Heatherly, J.A. Horton, L. Martinez, B. Campillo, Scripta Materialia 48 (2003) 185–190.
[25] V. Behrani, A.J. Thom, M.J. Kramer, M. Akinc, Intermetallics 14 (2006) 24–32.
[26] Y. Liu, M. Kramer, A. Thom, M. Akinc, Metallurgical and Materials Transactions A 36 (2005) 601–607.
[27] P.K. Ray, M. Akinc, M.J. Kramer, Journal of Alloys and Compounds 489 (2010) 357–361.
[28] A.R. Miedema, Journal of the Less Common Metals 46 (1976) 67–83.
[29] A.R. Miedema, F.R.d. Boer, P.F.d. Chatel, Journal of Physics F: Metal Physics 3 (1973) 1558–1576.
[30] A.R. Miedema, P.F. de Chatel, F.R. de Boer, Physica B+C 100 (1980) 1–28.
[31] A.R. Miedema, A.K. Niessen, Physica 114B (1982) 367–374.
[32] A.R. Miedema, A.K. Niessen, Calphad 7 (1983) 27–36.
[33] F.R.d. Boer, R. Boom, W.C.M. Mattens, A.R. Miedema, A.K. Niessen, Cohesion in Metals: Transition Metal Alloys North Holland, Amsterdam, 1988.
[34] H. Bakker, Enthalpies in Alloys: Miedema's Semi-empirical Model, Trans Tech Publications., Switzerland, 1998.
[35] A.K. Niessen, F.R. de Boer, R. Boom, P.F. de Chatel, W.C.M. Mattens, A.R. Miedema, Calphad 7 (1983) 51–70.
[36] G. Kresse, J. Furthmüller, Computational Materials Science 6 (1996) 15–50.
[37] H.J. Monkhorst, J.D. Pack, Physical Review B 13 (1976) 5188.
[38] B.H. Toby, Journal of Applied Crystallography 34 (2001) 210–213.
[39] T. Geng, C. Li, X. Zhao, H. Xu, Z. Du, C. Guo, Calphad 34 (2010) 363-376.
[40] H. Fujiwara, Y. Ueda, Journal of Alloys and Compounds 441 (2007) 168–173.
[41] I. Tomaszkiewicz, G.A. Hope, C.M. Beck Ii, P.A.G. O'Hare, The Journal of Chemical Thermodynamics 28 (1996) 29–42.
[42] A.K. McMahan, J.E. Klepeis, M. van Schilfgaarde, M. Methfessel, Physical Review B 50 (1994) 10742.
[43] A. Misra, J.J. Petrovic, T.E. Mitchell, Scripta Materialia 40 (1998) 191–196.
[44] C. Nunes, G. Coelho, A. Ramos, Journal of Phase Equilibria and Diffusion 22 (2001) 556–559.
[45] W.K. Wang, H. Iwasaki, C. Suryanarayana, T. Masumoto, N. Toyota, T. Fukase, F. Kogiku, Journal of Materials Science 17 (1982) 1523–1532.
[46] S.V.N. Naidu, A.M. Sriramamurthy, Si.W (Silicon–Tungsten), in: T.B. Massalski (Ed.), Binary Alloy Phase Diagrams, ASM International, 1990.